Desalination and Water Treatment
www.deswater.com

doi:10.5004/dwt.2021.27671

237 (2021) 241–250
October

Sorption of anionic dye by hybrid hydrotalcite/alginate beads in batch and in a fixed bed reactor

Lulu Zhao[a,b], Jean-Philippe Basly[b], Michel Baudu[b,*]

[a]*University of Science and Technology Liaoning, Tel. +33 (5)55 45 72 04; Fax: +33 (5)55 0000 00; email: luluzhao123@hotmail.com*
[b]*Université de Limoges, EA 4330 – Groupement de Recherche Eau Sol Environnement, 123 Avenue Albert Thomas, 87060 Limoges, France, emails: michel.baudu@unilim.fr (M. Baudu), jean-philippe.basly@unilim.fr (J.-P. Basly)*

Received 27 April 2021; Accepted 22 July 2021

ABSTRACT

The industrial applications of layered double hydroxides (LDH) in sorption processes have been, in certain cases, limited by nanometric/micrometric-sized particles. Herein, eco-friendly beads were prepared by encapsulating hydrotalcite into an alginate matrix in accordance with a gelation method using multivalent ions to avoid blocking the column membrane, for which a hydrotalcite with a different ratio of Mg/Al was synthesized. The analysis of sorption kinetics and isotherms in a batch reactor was performed for Methyl orange (MO) elimination. The LDH powder was analyzed before and after MO sorption by means of DRX and FIRT in order to confirm its structure and better understand the MO sorption mechanism. Results proved that hydrotalcite and hybrid hydrotalcite/alginate beads removed MO efficiently. However, the encapsulation process slightly decreased sorption capacity in the batch system and it was demonstrated that diffusion coefficients depended on bead size. Packed column experiments were also conducted, and the influence of flow rate and initial dye concentration on breakthrough curves were examined and simulated. The diffusion mechanism appeared to be a limiting factor within a dynamic system since the sorption capacity drastically declined, and the best fit to the experimental results was achieved by a diffusional model based on Fick's Second Law.

Keywords: Layered double hydroxides; Hybrid alginate beads; Methyl orange; Sorption; Diffusion mechanisms

1. Introduction

Because of the effect contaminated water can directly have on human health, adsorption is considered one of the most attractive technologies for eliminating pollutants from sewage. As a result, considerable effort has been devoted to developing effective methods of removing heavy metals [1], dye pollutants [2–6], and other organic pollutants [7] from wastewater.

Layered double hydroxides (LDHs) or hydrotalcite-like materials [8], as represented by the general formula $[M^{2+}_{1-x}M^{3+}_{x}(OH)_2]^{x+}[A^{m-}_{x/m}\cdot zH_2O]$, are easily produced using low-cost processes such as the co-precipitation technique. Their versatility in chemical compositions and physicochemical properties offer a wide array of applications in (photo)catalysis [9], anion sorption [10], and biological/pharmaceutical fields [8]. Among these materials, the Mg/Al LDH corresponds to a natural hydrotalcite and possesses a favorable sorption capacity for anions [11]. Despite this, industrial applications remain limited by the nanometric/micrometric-sized particle, and thus, different granulation techniques have become essential in LDH application. Among these methods, encapsulation is an economical and mild process, whereby the designated material is confined within a hydrogel to obtain millimetric granular hybrid beads.

The annual expenditure involved in industrial wastewater treatment is more than several billion dollars, and

---

* Corresponding author.

compared to other methods of wastewater purification, the cost of the adsorption technique is relatively low, especially for alginate application [12–14]. Alginate is an eco-friendly biopolymer that has already been somewhat in wastewater treatment [15] with easily reproducible efficacy [13]. To take advantage of these benefits, in this work, eco-friendly hybrid hydrogel beads were prepared by means of encapsulating Mg/Al LDH into an alginate matrix via a simple gelation method with multivalent ions. Among the many sources of pollution, dyes, such as Methyl orange and methylene blue, pose a particularly great threat to the environment. High concentrations of dye have been recognized for their impact on human and animal health [16]. Hence, Methyl orange (MO) a dye introduced as a probe molecule in sorption and catalysis studies, was chosen as the anionic species for this work. Sorption kinetics and isotherms in batch systems were studied to yield an in-depth understanding of Methyl orange sorption characteristics. Continuous flow conditions have been commonly used in industrial wastewater treatment due to their simplicity, ease of application, handling, and regeneration capacity while packed column experiments have also been carried out, and the influence of operational process parameters (i.e., flow rate and initial dye concentration) on breakthrough curves examined and simulated.

2. Materials and methods

2.1. Hydrotalcite-like materials

The hydrotalcite materials (LDHs) were synthesized by following a co-precipitation method [17] with NaOH/Na_2CO_3, using $Mg(NO_3)_2·6H_2O$ and $Al(NO_3)_3·9H_2O$ as the starting chemicals. The discrete 1:1 to 4:1 molar ratio of Mg/Al was prepared by varying the precursor's quantity and then labeling it as L1 to L4. Calcination was performed in an electric furnace at 550°C for 4 h. The crystalline structures before and after sorption were determined by X-ray diffraction (XRD) recorded on a Siemens D5000 X-ray powder diffractometer (CuKα radiation = 1.5418 Å; 2θ = 5°–70°). Fourier-transform infrared (FTIR) spectroscopy was conducted using a PerkinElmer Spectrum 65 in order to identify the functional groups present in the samples. The substance was finely ground and dispersed into KBr powder pressed pellets, and absorbance data was obtained over a range of wavenumbers from 4,000 to 400 cm^{-1}. Scanning electron microscopy (SEM) analysis of calcined and uncalcined LDH was conducted on a Philips XL 30 device using an acceleration voltage of 10 kV. Zeta potentials were measured in triplicate on a zeta photometer IV (CAD Instruments).

2.2. Hybrid beads

Hybrid beads were prepared using an ionic gelation method [18]. Hydrotalcite (LDH) (1% w/w) was dispersed in 100 mL of Milli-Q water, before an alginate suspension (medium viscosity) (1% w/w; V = 100 mL) was added, and the mixture (200 mL) was stirred for 2 h. The homogeneous mixture was forced through a micropipette tip by a peristaltic pump, and the resulting droplets were collected in a stirred reservoir containing 200 mL of 0.1 M $CaCl_2$. Two different bead sizes were obtained by modifying the end disposable tip diameter. After 24 h, the beads were filtered, washed several times with Milli-Q water and used immediately after preparation.

Apparent bead volumes and densities were measured by the volumetric displacement method and pycnometry (AccuPyc 1330 pycnometer), respectively. The shape of the hybrid beads was observed using a Motic BA200 digital camera attached to a Nikon optical microscope, and bead size was recorded by running ImageJ software. Composite beads were dried at 40°C until achieving a constant weight, and from there the experimental water content could be calculated.

2.3. Sorption experiments

Nonlinear regression analysis was performed using the STATISTICA 6.0 software package and suitability was assessed on the basis of correlation coefficient (R^2).

Methyl orange is an anionic dye within the pH range of this study, for which a stock solution of Methyl orange (abbreviated MO) was prepared in Milli-Q water, stored in the dark at 4°C until it was required and was used without further purification.

Kinetic studies in a batch system of the following were conducted at room temperature and without pH adjustment (pH = 5.5) by shaking: (i) 2.0 ± 0.1 g of hybrid beads; or (ii) 0.1 ± 0.01 g of powder hydrotalcite-like materials (LDHs), each with 100 mL of a solution containing MO (200 and 400 mg L^{-1}) at 200 rpm on a mechanical shaker (KS 501 digital - IKA). The samples were then withdrawn from the shaker at intervals ranging from 0 to 1,440 min. Residual MO concentrations were determined by UV-Visible spectrophotometry (VARIAN Cary UV) at 465 nm after filtration through a 0.45 μm membrane. Isotherms were determined at ambient temperature by shaking the materials (2.0 ± 0.1 g beads or 0.1 ± 0.01 g LDH powder) for 24 h in 100 mL of a solution containing MO (0–1,000 mg L^{-1}). Residual MO concentrations were identified in a manner as described in the kinetic study.

The continuous-flow experiments were carried out in a packed-bed reactor. The packed column has an inner diameter of 2.5 cm and a length of 30 cm and MO solutions were passed continuously and vertically through the column using a peristaltic pump, whose constant flow rate was frequently checked over the course of the experiments. Various sets of experiments were conducted to distinguish the effects of changes in concentration (5, 7.5, and 10 mg L^{-1}) and influent flow rate (0.015, 0.025, and 0.05 L h^{-1}). Samples from the column outlet were regularly collected by a programmed fraction collector and then analyzed by spectrophotometry at 465 nm.

3. Results and discussion

3.1. Hydrotalcite: characteristics and sorption properties

A preliminary survey was conducted regarding the sorption properties of hydrotalcite-like materials with an Mg/Al ratio varying from 1:1 to 4:1 (L1 to L4). Subsequently, the Langmuir model [Eq. (1)] was used to fit the experimental isotherm data:

$$q_e = q_m \frac{K_L C_e}{1 + K_L C_e} \tag{1}$$

where q_e, q_m, and C_e represent the MO adsorbed at equilibrium (mg g^{-1}), the maximum adsorption capacity (mg g^{-1}), and the MO concentration in solution at equilibrium (mg L^{-1}), respectively, while K_L corresponds to the Langmuir constant (L mg^{-1}).

The sorption capacity rose from 587 to 822 mg g$_{\text{HDL}}^{-1}$ as the Mg/Al ratio increased from 1:1 to 4:1 (as shown in Fig. 1 and Table 1). A similar evaluation was reported in previous work [19] for phosphate adsorption onto Mg/Al LDH, with the ability for phosphate adsorption increasing from 53.39 to 81.83 mg g^{-1} as the Mg/Al molar ratio rose from 2 to 4 [19]. This assumption was likely supported by the variation in zeta potential vs. molar ratio. For each molar ratio, the positive zeta potential, which favored the sorption of anionic species, was observed to be 3 mV (L1), 4 mV (L2) and 25 mV (L3, L4), respectively. Typically, calcination does not significantly influence zeta potential (22 for CLDH), thus, based on the results obtained, an Mg/Al ratio = 3 (i.e., L3) was selected for the hybrid bead syntheses.

The LDH structure was then examined by means of XRD (Fig. 2a). The patterns revealed sharp and symmetrical reflections at 2θ = 11.2°, 22.9°, and 34.6°, which were ascribed to the diffraction planes (003), (006), and (009) [20,21]. The lattice parameters for L3 were calculated for a hexagonal unit cell on the basis of the rhombohedral 3R1 structure. Parameter a [20] (0.35 nm = 2d$_{110}$) is correlated with the cation–cation distance within the brucite-like layer, while parameter c (2.41 nm = 3d$_{003}$) is correlated with the brucite-like layer thickness and the interlayer distance [20]. From this assessment, an interlayer free spacing was calculated by subtracting the brucite sheet thickness (0.480 nm) from the basal spacing d$_{003}$, yielding a distance of 0.324 nm [20]. The average crystallite sizes, upon applying the Debye–Scherrer relationship, were 6.8 nm (003) and 17.6 nm (110). Subsequently, the basal spacings d(003) for L1 to L4 were determined to be increasing from 7.69 to 8.04 Å over the range of Mg/Al ratios from 1 to 4. Moreover, the interlayer free spacing increased from 0.289 to 0.324 nm, that is, a change similar to that of the values observed earlier [22]. This additional interlayer spacing may correspond to another factor explaining the increase in sorption capacity with Mg/Al ratio. Notably, the d(003) of L3 increased from 8.04 to 8.12 Å after MO sorption, while the interlayer spacing changed from 0.324 to 0.332 nm, which was considered to be due to some MO ions being intercalated into the LDH interlayer by anion exchange with CO_3^{2-} [23]. Calcination led to the formation of mixed oxides as instanced when the layered structure disappeared after calcination [20], so the (200) and (220) reflections could be attributed to the mixed cubic MgO-like oxide [21]. However, the DRX patterns of CLDH after MO sorption became identical with those of L3. Consequently, it may be claimed that after calcination, the mixed oxides in solution were reversibly transformed back into the original double-layer structure, demonstrating the “memory effect” or ”reconstruction procedure” [24].

The hydrotalcite structure of L3 was also corroborated by FTIR (Fig. 2b). The vibrations at 3,420 and 1,650 cm^{-1} were assigned to the (OH) and δ(OH) modes, respectively [25,26]. The presence of carbonate was highlighted by the bands at 1,385; 665 and 870 cm^{-1} [25,26], while the bands close to 555 and 450 cm^{-1} were attributed to Al–OH and AlO_6^{3-},

Table 1
Isotherm studies. Langmuir parameters for L1 to L4 and LDH after calcination

Material	q_m (mg g^{-1})	K_L × 10^2 (L mg^{-1})	R^2
L1	587 ± 215	0.2 ± 0.1	0.98
L2	760 ± 147	0.3 ± 0.1	0.98
L3	827 ± 62	1.8 ± 0.3	0098
L4	822 ± 68	2.7 ± 0.5	0.99
CLDH	598 ± 116	0.3 ± 0.1	0.98

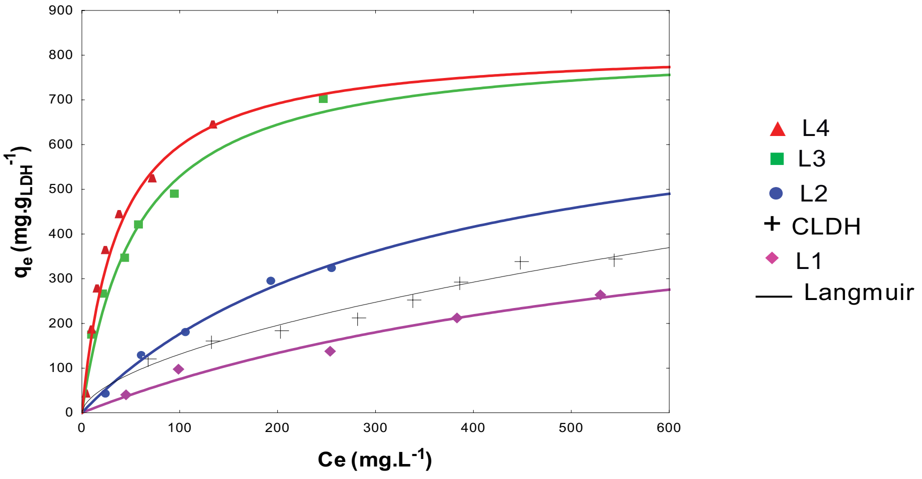

Fig. 1. Adsorption isotherms curves and Langmuir model parameters of Methyl orange. Operating conditions: ambient temperature; t = 24 h; m = 0.1 ± 0.01 g; [MO] = 0–1,000 mg L^{-1}; V = 100 mL. 1, 2, 3, 4 are corresponding to the Mg/Al ratio and CLDH to the calcined L3 material. The solid lines represent the fits with the Langmuir model.

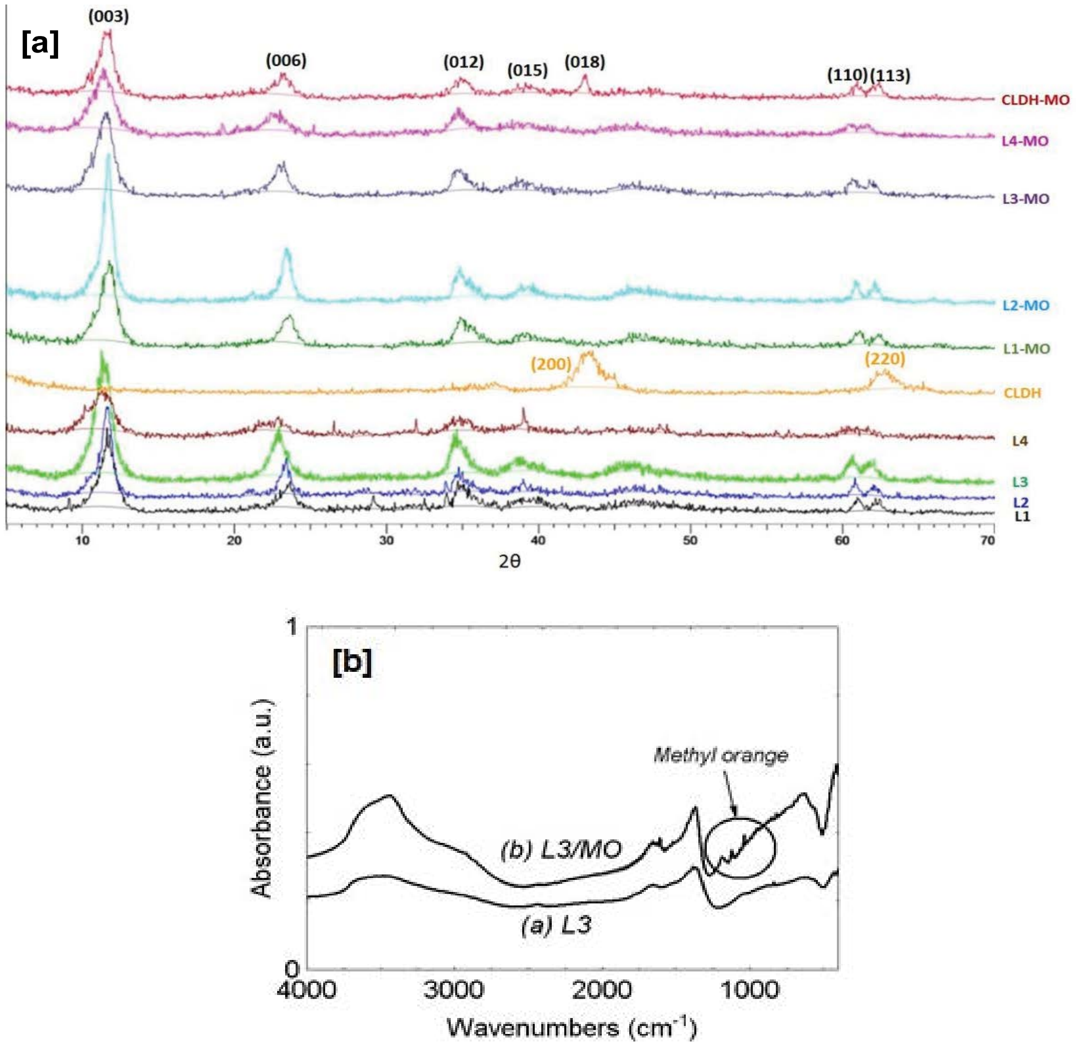

Fig. 2. [a] X-ray diffraction patterns of L1 to L4 and CLDH before and after MO sorption and [b] FTIR spectra (a) L3; (b) after Methyl orange sorption onto L3.

respectively [21]. The sorption of MO was suggested by the bands at 1,180; 1,115 and 995 cm^{-1} (Fig. 3b). The weak intensities of these bands across the FTIR spectrum were ascribed to the low MO concentration on the external surface of L3. The SEM analysis provided further evidence of the LDH structure (Fig. 3), and Fig. 3a confirms its sheet structure. After calcination (Fig. 3b), it became amorphous (as implied by the disappearance of the LDH structure) and more porous, which is in agreement with the results obtained by Lin et al. [27].

Fig. 1 shows that the calcination of LDH decreases their sorption capacity for MO, perhaps as a result of the disappearance of ion exchange sites between LDH interlayers. The MO sorption mechanism on LDH was probably implemented by the ion exchange between MO and CO$_3^{2-}$/OH$^-$ [23] as, after calcination, the amount of carbonate decreased, causing a drop in sorption capacity. A similar observation was obtained in an earlier study [28] for the phosphate sorption by LDH wherein after calcination, sorption capacity decreased from 45.3 to 11.5 mg g^{-1}.

3.2. Hybrid beads: sorption properties in batch systems

Spherical hybrid hydrotalcite (L3)/alginate beads (denoted by HHB$_{\text{size}}$) were prepared using two different end disposable tips. The average diameters of the beads produced from these tips were 2.9 and 4.6 mm, with a density of 1.01 g cm^{-3} and experimental water content of 96%.

Kinetic studies, along with a set of experiments, were completed in order to explore the effect of various operating conditions: encapsulation; initial concentration; contact time; and bead size. The reaction equilibrium was reached at 8–10 h and results were in good agreement with a pseudo-second-order model as below:

$$q_t = \frac{q_e^2 k_2 t}{1 + q_e k_2 t} \tag{2}$$

where q_e represents the amount of pollutant adsorbed at equilibrium (mg g^{-1}), q_t the amount of pollutant adsorbed at time t (mg g^{-1}), and k_2 the pseudo-second-order rate constant (g mg^{-1} min^{-1}). The sorption parameters appeared to be dependent on both initial concentration and bead size (Table 2).

Sorption implies that the reaction has occurred in the presence of a diffusion mechanism at the hydrotalcite surface. Effective diffusion coefficients (D_e) could be obtained from experimental data according to the procedure given by Reichenberg [29]:

$$F(t) = \frac{q_t}{q_e} = 1 - \frac{6}{\pi^2}\sum_{n^2}^{\infty}\frac{1}{n^2}\exp\left(-\frac{n^2\pi^2}{R_p^2}D_e t\right) \quad (3)$$

By means of Fourier transform application and integration, Reichenberg derived the following approximation for $F(t) < 0.85$:

$$B \cdot t = \left(\sqrt{\pi} - \sqrt{\pi - \frac{\pi^2 F(t)}{3}}\right)^2 \quad (4)$$

which features the substitution $B = D_e(\pi^2/R_p^2)$, where R_p is the bead radius (m), and D_e is the diffusion coefficients. From Eq. (3), q_e and q_t represent the amounts of pollutant adsorbed at equilibrium and at time t (mg g^{-1}), respectively.

The plots of $B \cdot t$ vs. time are shown in Fig. 4, whose linearity and zero Y-intercept value indicate that the mass transfer process was controlled by internal diffusion [29].

The diffusion coefficient, as determined under various conditions, is presented in Table 2. A significant increase in both the diffusion coefficient and kinetic constant was observed with the use of a larger bead size. This finding can be explained by the greater amount of water in the 4.6 mm beads than as contained in the 2.9mm beads, with a hydrogel whose properties are very similar to those of water. The diffusion coefficient in water is normally greater than that of hydrogel and as per previous work [30], this property of vitamin B_{12} in water was shown to be between twice or three times greater than as in alginate gel. Furthermore, the kinetic constant decreased significantly upon encapsulation, an observation that was concluded to be due to the presence of alginate gel, which could potentially limit the contact between MO and LDH inside the beads.

In accordance with previous kinetic studies, the equilibrium time adopted for the isotherms was set at 24 h. The analysis of equilibrium isotherms was critical and the data obtained with HHB provided an adequate fit with the Langmuir model. In contrast, no MO sorption was observed when alginate beads (AB) were used (Table 3), hence, the sorption property was only associated with LDH inside the beads and the sorption parameters were applied to the LDH mass inside the hydrogel.

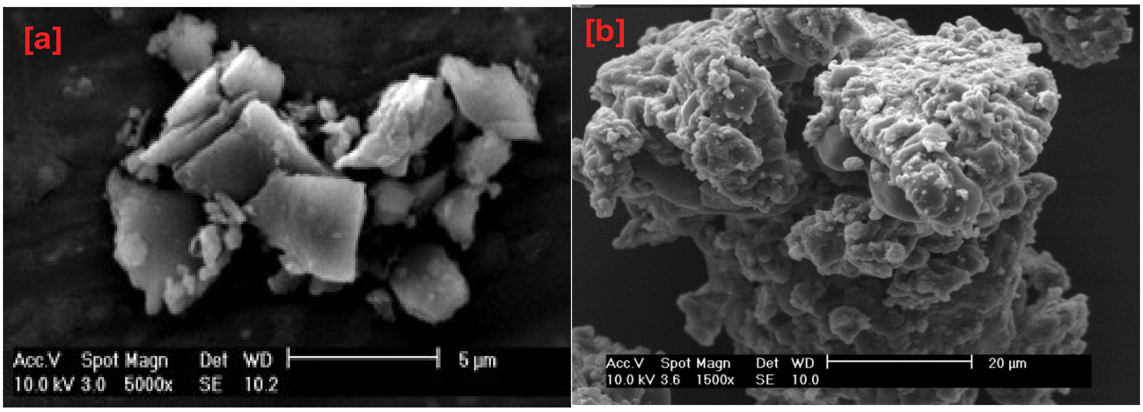

Fig. 3. SEM analyses for L3 before (a) and after calcination (b).

Table 2
Spherical hybrid hydrotalcite (L3)/alginate beads. Kinetic studies in batch systems: pseudo-second-order and homogeneous diffusion coefficients

Materials	C (mg L^{-1})	Pseudo-second-order		Reichenberg	
		k_2 (g mg^{-1} min^{-1})	R^2	D_e (m^2 s^{-1})	R^2
L3	400	(5.4 ± 1.1) × 10^{-4}	0.98	n.d.	n.d.
HHB$_{2.9}$	400	(1.5 ± 0.4) × 10^{-5}	0.99	(2.6 ± 0.2) × 10^{-11}	0.96
HHB$_{2.9}$	200	(3.4 ± 0.8) × 10^{-5}	0.98	(1.0 ± 0.1) × 10^{-11}	0.99
HHB$_{4.6}$	400	(1.1 ± 0.2) × 10^{-4}	0.98	(8.9 ± 0.2) × 10^{-11}	0.98
HHB$_{4.6}$	200	(5.6 ± 0.9) × 10^{-5}	0.99	(2.6 ± 0.1) × 10^{-11}	0.97

HHB: Spherical hybrid hydrotalcite (L3)/alginate beads. 2.9 and 4.6 are the diameter (mm) of the spherical beads;
m = 2.0 ± 0.1 g; [MO] = 200, 400 mg L^{-1}; V = 100 mL; T = ambient; t = 0–24 h.

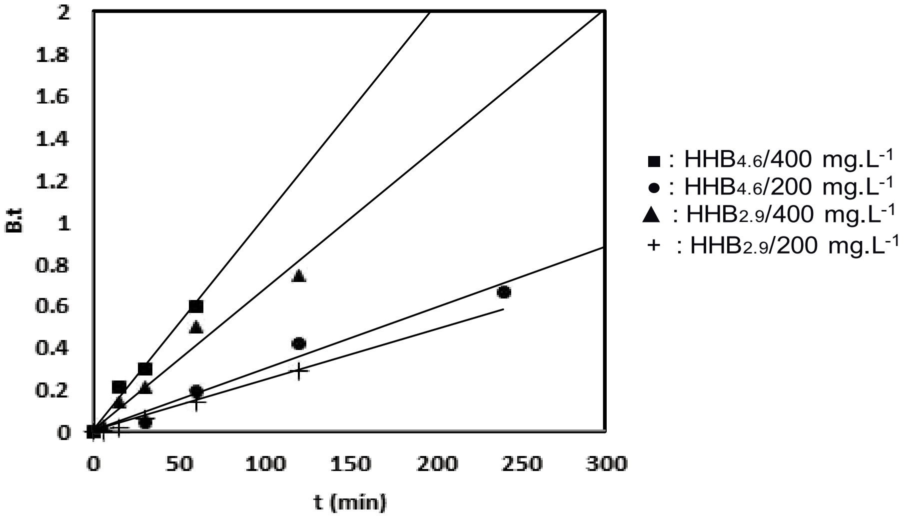

Fig. 4. Homogeneous diffusion coefficients determination. The solid lines represent the fits with the Reichenberg equation.

Table 3
Isotherm studies. Langmuir parameters for alginate beads (AB), L3 and HHB

Material	q_e (mg g^{-1})	K_L × 10^2 (L mg^{-1})	R^2
L1	587 ± 215	0.2 ± 0.1	0.98
L2	760 ± 147	0.3 ± 0.1	0.98
L3	827 ± 62	1.8 ± 0.3	0098
L4	822 ± 68	2.7 ± 0.5	0.99
AB	0	n.d.	n.d.
$HHB_{2.9}$	766 ± 42	0.6 ± 0.1	0.99
$HHB_{4.6}$	753 ± 45	0.5 ± 0.1	0.99

This result showed that sorption capacity decreases with encapsulation (Table 3). As with the kinetic studies, alginate gel limits MO dispersion and MO molecules cannot access the entire reactive surface of LDH nanoparticles. The Langmuir constant decreases slightly with bead size, a possible cause being that the smaller beads allowing for solute diffusion on a larger fraction of the three-dimensional gel, particularly in the middle of the bead. To better understand the sorption mechanism in both LDH and HHB, a mechanism diagram is presented in Fig. 5. MO sorption on LDH was achieved by an anion exchange between the MO molecule and CO_3^{2+}, along with the external surface sorption on LDH [23]. For HHB, sorption was initiated by MO molecule diffusion in the alginate gel and then fixed by LDH inside the beads.

The maximum removal efficiency towards MO with some of the materials studied in the literature is compared in Table 4 [31–36], and this capability was much higher in L3 and HHB than in the organic–inorganic composite. Among the hydrotalcite-like materials, L3 (Mg/AlLDH) appears to be one of the best materials for removing MO.

3.3. Hybrid beads: sorption properties in a dynamic system

$HHB_{2.9}$ was used in packed bed columns, for which the breakthrough curves are plotted in Fig. 6. The effects of two variables, the superficial velocity via flow rate modification (0.015, 0.025, and 0.05 L h^{-1}; Fig. 6a), and MO concentration (5, 7.5, and 10 mg L^{-1}; Fig. 6b), were investigated, while the experimental sorption capacity or adsorbed MO quantity q_{exp} was calculated by using Eq. (5):

$$q_{\text{exp}} = QC_0 \int_{t=0}^{t=\text{total}} \left(1 - \frac{C_t}{C_0}\right) dt \tag{5}$$

As shown in Fig. 6a, the breakthrough curves become steeper with increasing flow rate, while a decrease in flow rate from 0.1 to 0.03 m h^{-1} increases sorption capacity from 12.8 to 18.4 mg g^{-1} (Table 5). These improvements were possible due to the longer contact time between adsorbate and adsorbent, behavior that could be explained by the fact that sorption was affected by solute residence time in the column, solute diffusion into the pores, and limited access to the active sites.

As expected, increasing the initial MO concentration from 5 to 10 mg L^{-1} raised the sorption capacity q_{exp} from 14.5 to 38 mg g^{-1} (Table 5), a trend that matches sorption in batch systems, where sorption capacity increased from 18 to 37 mg g^{-1} across the same range of MO concentrations. This trend was also confirmed by results recorded in literature [37].

The Thomas model [Eq. (6)] was then used to describe the breakthrough curves. This model relies on the Langmuir isotherm for equilibrium and second-order reversible reaction kinetics. It assumes a constant separation factor but is applicable under both favorable and unfavorable sorption conditions, thus being suitable for sorption processes devoid of external and internal diffusion limitations.

$$\frac{C}{C_0} = \frac{1}{1 + \exp\left(\frac{k_T q_0 m}{Q} - k_T C_0 t\right)} \tag{6}$$

In Eq. (6), k_T is the Thomas rate constant (mL h^{-1} mg^{-1}), q_0 the equilibrium uptake capacity (mg g^{-1}), m the mass of sorbent packed in the column (g), and Q the volumetric flow rate (L h^{-1}). C and C_0 are the MO concentrations (mg L^{-1}) in the effluent and influent at time t (h), respectively. Table 5 lists the calculated Thomas constants from the experimental data.

These results suggest that better column sorption is the result of a higher MO concentration (C_0) but with a lower feed flow rate (u). The adsorbed quantity in the column was lower than the values predicted by sorption isotherms, which was conjectured to be caused by an equilibrium not being reached in the fixed-bed reactor.

The comparison between capacities determined by the Thomas model (q_0) and calculated capacities (q_{exp}) revealed a poor description of some experiments (Table 5). From

Table 4
Comparison of sorption maximum capacities of various adsorbents for MO

Materials	Maximum capacity (mg g^{-1})	Reference
Activated carbon	217	[31]
MgO/chitosan composite	60	[32]
LDH Ni/Fe	206	[33]
LDH Zn/Al calcined	200	[34]
LDH Co/Fe	1219	[35]
γ-Fe_2O_3/Carbon/Chitosan	61-66	[36]
L3	827	This study
$HHB_{2.9}$	766	This study

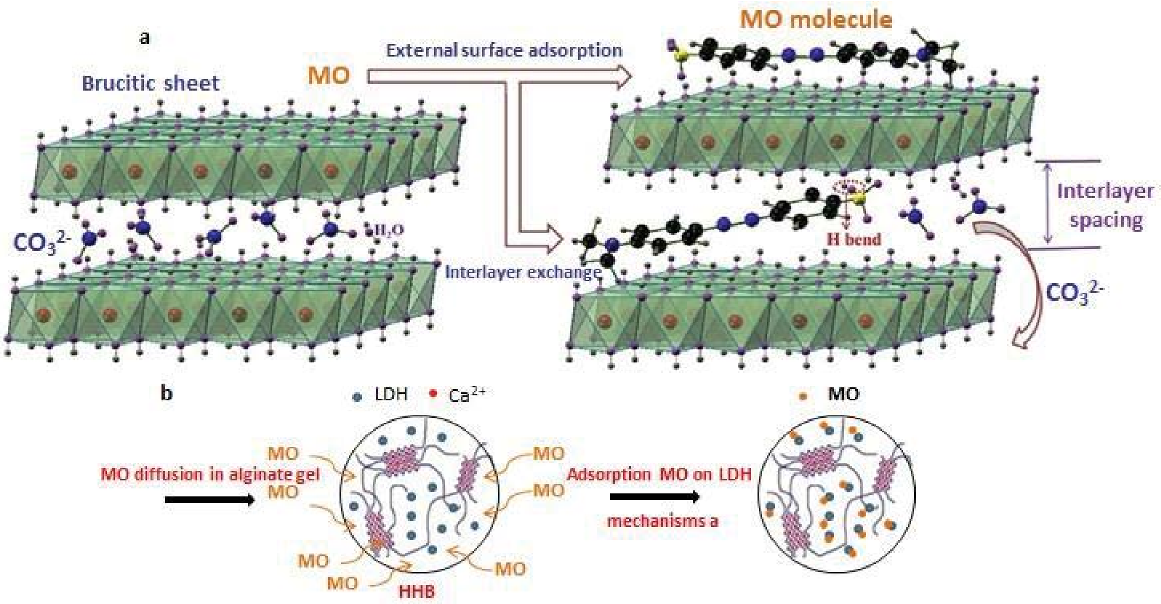

Fig. 5. MO sorption mechanism on (a) LDH [19] and (b) HHB.

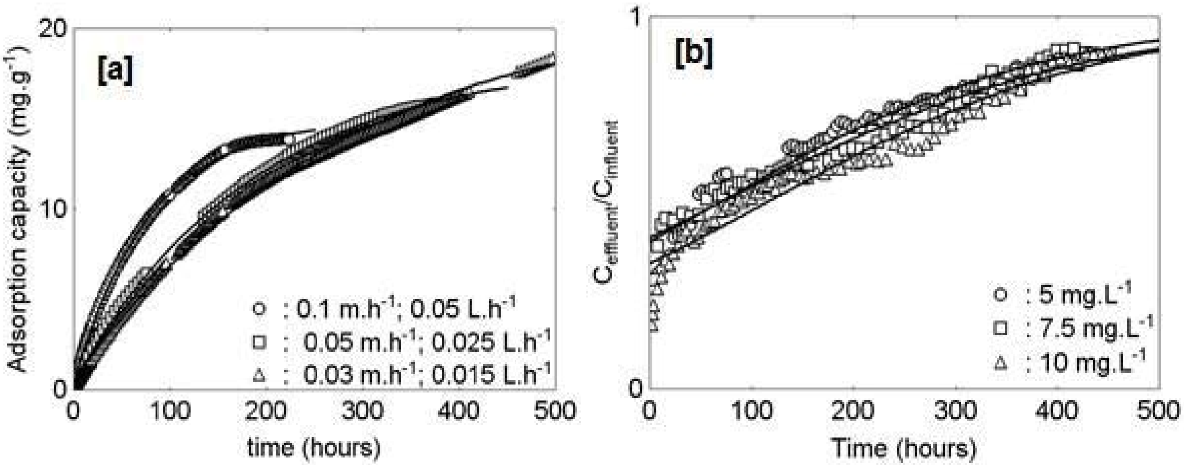

Fig. 6. Experimental and simulated (solid lines) breakthrough curves. [a] Influence of flow rate and [b] influence of initial Methyl orange concentration. The simulated curves were calculated from the Thomas model.

this observation, a simple diffusional equation, based on Fick's Second Law and previously employed to model diffusion processes in biopolymeric networks [38], was used to derive Eq. (7), which predicts how diffusion causes the concentration to change over time. For simple geometrical cases (spheres in our case), the equation is modified to become Eq. (8):

$$q_t = q_e\left(1 - b\exp\left(-k \cdot t\right)\right) \tag{7}$$

With

$$q_t = QC_0 \int_{t=0}^{t} \left(1 - \frac{C_t}{C_0}\right) dt \tag{8}$$

where q_t is the sorption capacity at time t obtained by integrating the experimental breakthrough curves with respect to time (mg g^{-1}), q_e the sorption capacity at equilibrium (mg g^{-1}), k the mass transfer coefficient (m h^{-1}), and b a coefficient based on experimental conditions.

The Fick's Law model yielded good predictive ability for the breakthrough curves, as illustrated by the goodness-of-fit between the model and experimental data (Fig. 7, Table 5). However, Fick's Law does seem to overestimate the sorption capacities at equilibrium. Even so, the concentration affected sorption capacity as shown where the breakthrough curve did not significantly change with initial concentration since the adsorbed amount increased linearly in the range of the concentrations used. The low flow rate resulted in improved reactor performance thanks to the increased solution residence time within the column.

4. Conclusion

This work has explored the sorption capabilities of Mg/Al powder LDH and the LDH trapped in alginate beads towards anionic species (the exemplar in this study being Methyl orange, MO). Results have shown that the MO removal efficiency of the LDH powder and hybrid beads is quite high. The sorption capacity increased with Mg/Al molar ratio due to a widening of the LDH interlayer space, but decreased after calcination of LDH, a result of disappearing ion-exchange sites. Encapsulation in a hydrogel matrix implies that the sorption reaction occurs in the presence of a diffusion mechanism. diffusion coefficients were determined by following the procedure detailed by Reichenberg and were found to depend on both the beads' concentration and their size. Bead encapsulation was shown

Table 5
Column data with Thomas and Fick models parameters for MO sorption on the hybrid hydrotalcite beads with a diameter of 2.9 mm (HHB$_{2.9}$) and height of 0.15 m under different conditions

				Thomas model			Diffusional equation: Fick model			
u (m h^{-1})	C_0 (mg L^{-1})	q_{exp} (mg g^{-1})	q_{batch} (mg g^{-1})	q_0 (mg g^{-1})	$k_T \times 10^3$ (L h^{-1} mg^{-1})	R^2	q_0 (mg g^{-1})	$k \times 10^3$ (m h^{-1})	b	R^2
0.1	5	12.8	18 ± 3	11.6 ± 1.0	2.50 ± 0.07	0.972	15.8 ± 0.1	12.0 ± 0.1	0.98 ± 0.01	0.999
0.05	5	14.5	18 ± 3	13.5 ± 0.6	1.21 ± 0.03	0.981	18.4 ± 0.1	5.28 ± 0.05	0.98 ± 0.01	0.999
0.03	5	18.4	18 ± 3	17.5 ± 0.3	1.37 ± 0.04	0.938	21.7 ± 0.2	3.56 ± 0.06	0.98 ± 0.01	0.999
0.05	7.5	29.7	28 ± 4	19.1 ± 1.1	0.76 ± 0.03	0.965	26.9 ± 0.4	5.35 ± 0.18	1.00 ± 0.01	0.995
0.05	10	38	37 ± 6	35.4 ± 1.1	0.56 ± 0.02	0.981	41.6 ± 0.5	5.29 ± 0.16	1.00 ± 0.01	0.995

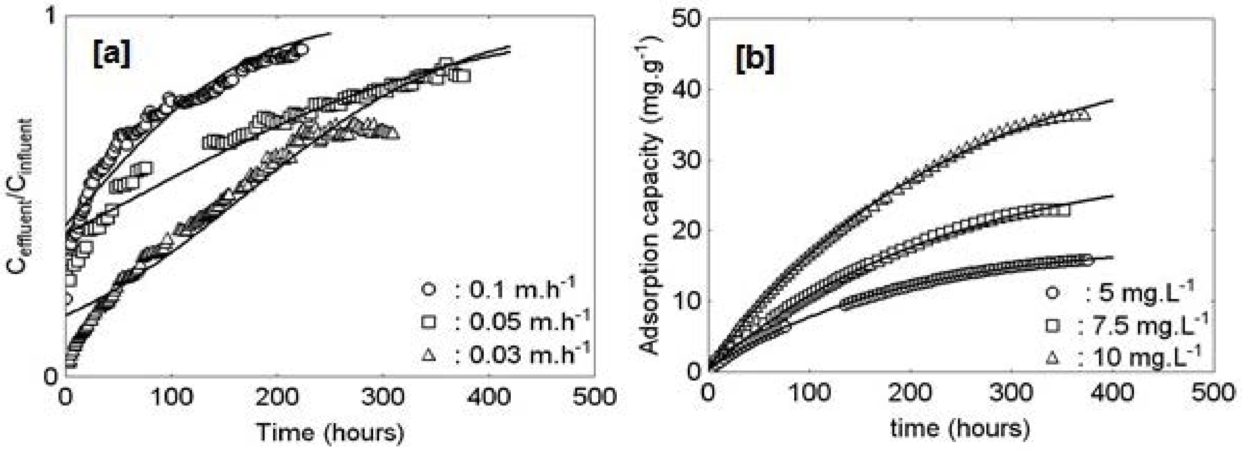

Fig. 7. Experimental and simulated (solid lines) fixed bed sorption capacities vs. time. [a] Influence of flow rate and [b] influence of initial Methyl orange concentration. The simulated curves were calculated from the diffusional model based on Fick's law.

to decrease the kinetic constant and sorption capacity. MO can be entirely eliminated in a continuous system since results demonstrated that the lower flow rate and higher initial MO concentration led to greater sorption in the column. The diffusion mechanism appears to be a limiting factor in a dynamic system since the sorption capacity was drastically diminished by comparison, and the best fit to experimental results was achieved by a diffusional model based on Fick's Second Law.

Acknowledgments

The authors would like to thank the Aquitaine-Limousin-Poitou-Charentes Region for its financial support of a Ph.D. program related to this work. The University of Science and Technology Liaoning youth project greatly appreciates their contribution.

References

[1] I. Anastopoulos, A. Mittal, M. Usman, J. Mittal, G. Yu, A. Núñez-Delgado, M. Kornaros, A review on halloysite-based adsorbents to remove pollutants in water and wastewater, J. Mol. Liq., 269 (2018) 855–868.

[2] C. Arora, S. Soni, S. Sahu, J. Mittal, P. Kumar, P.K. Bajpai, Iron based metal organic framework for efficient removal of methylene blue dye from industrial waste, J. Mol. Liq., 284 (2019) 343–352.

[3] V.K. Gupta, S. Agarwal, R. Ahmad, A. Mirza, J. Mittal, Sequestration of toxic congo red dye from aqueous solution using ecofriendly guar gum/activated carbon nanocomposite, Int. J. Biol. Macromol., 158 (2020) 1310–1318.

[4] A. Mariyam, J. Mittal, F. Sakina, R.T. Baker, A.K. Sharma, A. Mittal, Efficient batch and fixed-bed sequestration of a basic dye using a novel variant of ordered mesoporous carbon as adsorbent, Arabian J. Chem., 14 (2021) 103186, doi: 10.1016/j.arabjc.2021.103186.

[5] A. Mariyam, J. Mittal, F. Sakina, R.T. Baker, A.K. Sharma, Adsorption behaviour of Chrysoidine R dye on a metal/halide-free variant of ordered mesoporous carbon, Desal. Water Treat., 223 (2021) 425–433.

[6] L. Zhao, J.-P. Basly, M. Baudu, Macroporous alginate/ferrihydrite hybrid beads used to remove anionic dye in batch and fixed-bed reactors, J. Taiwan Inst. Chem. Eng., 74 (2017) 129–135.

[7] I. Anastopoulos, L. Pashalidis, A.G. Orfanos, L.D. Manariotis, T. Tatarchuk, L. Sellaoui, A. Bonilla-Petriciolet, A. Mittal, A. Núñez-Delgado, Removal of caffeine, nicotine and amoxicillin from (waste)waters by various adsorbents. A review, J. Environ. Manage., 261 (2020) 110236, doi: 10.1016/j.jenvman.2020.110236.

[8] D.G. Evans, X. Duan, Preparation of layered double hydroxides and their applications as additives in polymers, as precursors to magnetic materials and in biology and medicine, Chem. Commun., (2006) 485–496, doi: 10.1039/B510313B.

[9] G. Centi, S. Perathoner, Catalysis by layered materials: a review, Microporous Mesoporous Mater., 107 (2008) 3–15.

[10] R. Shan, L. Yan, Y. Yang, K. Yang, S. Yu, H. Yu, B. Zhu, B. Du, Highly efficient removal of three red dyes by adsorption onto Mg–Al-layered double hydroxide, J. Ind. Eng. Chem., 21 (2015) 561–568.

[11] K.-H. Goh, T.-T. Lim, Z. Dong, Application of layered double hydroxides for removal of oxyanions: a review, Water Res., 42 (2008) 1343–1368.

[12] A. Kolbasov, S. Sinha-Ray, A.L. Yarin, B. Pourdeyhimi, Heavy metal adsorption on solution-blown biopolymer nanofiber membranes, J. Membr. Sci., 530 (2017) 250–263.

[13] D. Wu, Y. Gao, W. Li, X. Zheng, Y. Chen, Q. Wang, Selective adsorption of La^{3+} using a tough alginate-clay-poly(n-isopropylacrylamide) hydrogel with hierarchical pores and reversible re-deswelling/swelling cycles, ACS Sustainable Chem. Eng., 4 (2016) 6732–6743.

[14] S. Soni, P. Kumar Bajpai, D. Bharti, J. Mittal, C. Arora, Removal of crystal violet from aqueous solution using iron based metal organic framework, Desal. Water Treat., 205 (2020) 386–339.

[15] A. Chatterjee, S. Schiewer, Multi-resistance kinetic models for biosorption of Cd by raw and immobilized citrus peels in batch and packed-bed columns, Chem. Eng. J., 244 (2014) 105–116.

[16] M.B. Kurade, T.R. Waghmode, S.M. Patil, B.-H. Jeon, S.P. Govindwar, Monitoring the gradual biodegradation of dyes in a simulated textile effluent and development of a novel triple layered fixed bed reactor using a bacterium-yeast consortium, Chem. Eng. J., 307 (2017) 1026–1036.

[17] Q. Tao, Y. Zhang, X. Zhang, P. Yuan, H. He, Synthesis and characterization of layered double hydroxides with a high aspect ratio, J. Solid State Chem., 179 (2006) 708–715.

[18] A. Ely, M. Baudu, M.O.S.O. Kankou, J.-P. Basly, Copper and nitrophenol removal by low cost alginate/Mauritanian clay composite beads, Chem. Eng. J., 178 (2011) 168–174.

[19] R. Li, J. Wang, B. Zhou, M. Awasthi, A. Ali, Z. Zhang, L. Gaston, A. Lahori, A. Mahar, Enhancing phosphate adsorption by Mg/Al layered double hydroxide functionalized biochar with different Mg/Al ratios, Sci. Total Environ., 559 (2016) 121–129.

[20] N. Das, R. Das, Insertion of chromium(III) ascorbate complex into layered double hydroxide through reduction of intercalated chromate by ascorbic acid, Appl. Clay Sci., 42 (2008) 90–94.

[21] H.-Y. Zeng, S. Xu, M.-C. Liao, Z.-Q. Zhang, C. Zhao, Activation of reconstructed Mg/Al hydrotalcites in the transesterification of microalgae oil, Appl. Clay Sci., 91–92 (2014) 16–24.

[22] D. Wan, Y. Liu, S. Xiao, J. Chen, J. Zhang, Uptake fluoride from water by caclined Mg-Al-CO_3 hydrotalcite: Mg/Al ratio effect on its structure, electrical affinity and adsorptive property, Colloids Surf., A, 469 (2015) 307–314.

[23] F. Ling, L. Fang, Y. Lu, J. Gao, F. Wu, M. Zhou, B. Hu, A novel CoFe layered double hydroxides adsorbent: high adsorption amount for Methyl orange dye and fast removal of Cr(VI), Microporous Mesoporous Mater., 234 (2016) 230–238.

[24] F. Cavani, F. Trifirò, A. Vaccari, Hydrotalcite-type anionic clays: preparation, properties and applications, Catal. Today, 11 (1991) 173–301.

[25] M. del Arco, C. Martin, I. Martin, V. Rives, R. Trujillano, A FTIR spectroscopic study of surface acidity and basicity of mixed Mg, Al-oxides obtained by thermal decomposition of hydrotalcite, Spectrochim. Acta, Part A, 49 (1993) 1575–1582.

[26] H. Laguna, S. Loera, I.A. Ibarra, E. Lima, M.A. Vera, V. Lara, Azoic dyes hosted on hydrotalcite-like compounds: non-toxic hybrid pigments, Microporous Mesoporous Mater., 98 (2007) 234–241.

[27] Y. Lin, Q. Fang, B. Chen, Perchlorate uptake and molecular mechanisms by magnesium/aluminum carbonate layered double hydroxides and the calcined layered double hydroxides, Chem. Eng. J., 237 (2014) 38–46.

[28] P. Koilraj, S. Kannan, Aqueous fluoride removal using ZnCr layered double hydroxides and their polymeric composites: batch and column studies, Chem. Eng. J., 234 (2013) 406–415.

[29] F.J. García-Mateos, R. Ruiz-Rosas, M.D. Marqués, L.M. Cotoruelo, J. Rodríguez-Mirasol, T. Cordero, Removal of paracetamol on biomass-derived activated carbon: modeling the fixed bed breakthrough curves using batch adsorption experiments, Chem. Eng. J., 279 (2015) 18–30.

[30] J.M.C. Puguan, X. Yu, H. Kim, Diffusion characteristics of different molecular weight solutes in Ca–alginate gel beads, Colloids Surf., A, 469 (2015) 158–165.

[31] S. Chen, J. Zhang, C. Zhang, Q. Yue, Y. Li, C. Li, Equilibrium and kinetic studies of Methyl orange and methyl violet adsorption on activated carbon derived from *Phragmites australis*, Desalination, 252 (2010) 149–156.

[32] Y. Haldorai, J.-J. Shim, An efficient removal of Methyl orange dye from aqueous solution by adsorption onto chitosan/MgO composite: a novel reusable adsorbent, Appl. Surf. Sci., 292 (2014) 447–453.

[33] Y. Lu, B. Jiang, L. Fang, F. Ling, J. Gao, F. Wu, X. Zhang, High performance NiFe layered double hydroxide for Methyl orange dye and Cr(VI) adsorption, Chemosphere, 152 (2016) 415–422.

[34] Z.-M. Ni, S.-J. Xia, L.-G. Wang, F.-F. Xing, G.-X. Pan, Treatment of Methyl orange by calcined layered double hydroxides in aqueous solution: adsorption property and kinetic studies, J. Colloid Interface Sci., 316 (2007) 284–291.

[35] F. Ling, L. Fang, Y. Lu, J. Gao, F. Wu, M. Zhou, B. Hu, A novel CoFe layered double hydroxides adsorbent: high adsorption amount for Methyl orange dye and fast removal of Cr(VI), Microporous Mesoporous Mater., 234 (2016) 230–238.

[36] H.Y. Zhu, R. Jiang, L. Xiao, G.M. Zeng, Preparation, characterization, adsorption kinetics and thermodynamics of novel magnetic chitosan enwrapping nanosized γ-Fe_2O_3 and multi-walled carbon nanotubes with enhanced adsorption properties for Methyl orange, Bioresour. Technol., 101 (2010) 5063–5069.

[37] J. Samuel, M. Pulimi, M.L. Paul, A. Maurya, N. Chandrasekaran, A. Mukherjee, Batch and continuous flow studies of adsorptive removal of Cr(VI) by adapted bacterial consortia immobilized in alginate beads, Bioresour. Technol., 128 (2013) 423–430.

[38] F.-N. Allouche, E. Guibal, N. Mameri, Preparation of a new chitosan-based material and its application for mercury sorption, Colloids Surf., A, 446 (2014) 224–232.